

Article

A Study of the Effects of Medical Dental Laser and Diamond Drill on Dentin Tissue during Dental Restoration Based on Spectral Imaging and Multivariate Analysis of Synchrotron FTIR Microspectroscopy Data

Pavel Seredin ^{1,*}, Dmitry Goloshchapov ¹, Nikita Buylov ¹, Dmitry Nesterov ¹, Vladimir Kashkarov ¹, Yuri Ippolitov ², Ivan Ippolitov ², Sergey Kuyumchyan ³ and Jitraporn Vongsvivut ⁴

¹ Solid State Physics and Nanostructures Department, Voronezh State University, University sq.1, 394018 Voronezh, Russia; goloshchapov@phys.vsu.ru (D.G.); kashkarov@phys.vsu.ru (V.K.)

² Department of Pediatric Dentistry with Orthodontia, Voronezh State Medical University, Studentcheskaya st. 11, 394006 Voronezh, Russia

³ Saint Petersburg State University Hospital, 154, Fontanka River Embankment, 198103 St. Petersburg, Russia

⁴ Australian Synchrotron (Synchrotron Light Source Australia Pty Ltd.), 800 Blackburn Rd, Clayton, VIC 3168, Australia

* Correspondence: paul@phys.vsu.ru

Abstract: In our work, the effect of a dental Er:YAG pulsed laser and a diamond cylindrical drill with a turbine handpiece on dentin tissue was studied using spectral imaging. The combination of spectral imaging of FTIR microspectroscopy data and subsequent multivariate analysis (hierarchical cluster analysis (HCA) and principal component analysis (PCA)) was shown to unambiguously detect visually indistinguishable structural changes occurring in the hard dental tissue (dentin) depending on the method used for their pre-processing, and to classify and differentiate the identified features at the submicron level with high spatial resolution. The detectable spectral transformations indicate that the preparation of dental tissue with a dental laser leads to significant changes in the organic components of dentin, which may affect adhesion. The use of a diamond cylindrical drill with a turbine handpiece is characterized by a larger area (depth) of the altered hard tissue than in the case of a dental laser for dental cavity preparation. The observed redistribution of the phase composition of the inorganic component in the tissue is associated with the emergence of additional phases of weak calcium phosphates, and changes in the organic component with transformations in the secondary structure of proteins. Active use of the proposed integrated approach in the future will clarify the areas of its applicability to the analysis of biological tissues and pathologies in them, which will help in the clinical setting to choose the optimal personalized approach for patients.

Keywords: spectral imaging; FTIR microspectroscopy; dental tissue; dental laser; diamond drill



Citation: Seredin, P.; Goloshchapov, D.; Buylov, N.; Nesterov, D.; Kashkarov, V.; Ippolitov, Y.; Ippolitov, I.; Kuyumchyan, S.; Vongsvivut, J. A Study of the Effects of Medical Dental Laser and Diamond Drill on Dentin Tissue during Dental Restoration Based on Spectral Imaging and Multivariate Analysis of Synchrotron FTIR Microspectroscopy Data. *Photonics* **2023**, *10*, 881.

<https://doi.org/10.3390/photonics10080881>

Received: 25 April 2023

Revised: 8 July 2023

Accepted: 27 July 2023

Published: 28 July 2023



Copyright: © 2023 by the authors. Licensee MDPI, Basel, Switzerland. This article is an open access article distributed under the terms and conditions of the Creative Commons Attribution (CC BY) license (<https://creativecommons.org/licenses/by/4.0/>).

1. Introduction

Data visualization has an important place in modern medicine. The advanced processing of medical images and biosignals allows not only for the diagnosis of diseases, but also for the selection and adjustment of the necessary measures required to plan a patient's treatment.

For a long time, two-dimensional imaging techniques have been used in medicine, and are still used in practice [1]. However, the development of diagnostic technologies led to the emergence of 3D volumetric imaging (tomography) techniques, which was a breakthrough in the subject area. For example, an unprecedented combination of resolution and contrast in imaging caries in vitro can be obtained using synchrotron microcomputed tomography [2]. However, it is necessary to solve a number of parallel problems associated with combining and analyzing a large number of two-dimensional images.

Another technology that has recently come into use is spectral imaging (spectral image), which is actively used in applied scientific research but is still rarely used in medical diagnostics [3,4]. In this approach, using micro and often nanoscopic methods to obtain an image, one or another spectral method is used simultaneously to collect an array of spectral data (pointwise) [4].

For medical diagnostic tasks, the most convenient form of spectral imaging is to combine the techniques of molecular spectroscopy and optical or probe microscopy into a single diagnostic scheme, which allows for the analysis of biological samples without irreversible external influences [5–7]. Using the characteristic signatures of molecular spectroscopy (position, width and shape of the spectral line) chemical/molecular images of the micro/nano region of the sample being diagnosed can be collected and its nature established [8,9]. Subsequent application of multivariate analysis techniques to the large spectral dataset collected allows for the extraction of principle information useful for accurate and rapid monitoring of molecular specific distribution in biotissues, or, for example, the bacterial status in the analyzed area [10–12].

High-resolution spatial spectral imaging at the micro- and nanoscale may be the key to new principles of disease prevention and treatment [2,12,13]. The visibility, sensitivity, and rapidness of such a diagnostic tool are the main criteria for its applicability to the analysis of objects of a biological nature.

This technique has previously been shown to be promising when FTIR microspectroscopy was used for spectral imaging of biological tissues (dental tissue) as well as the pathological processes occurring in them [11,14,15]. The combination of synchrotron radiation and FTIR-microspectroscopy made it possible to achieve lateral resolution in the micron range, which exceeds (by an order of magnitude) the resolution of laboratory FTIR instruments [10,11,14,16–18]. This approach made it possible to not only collect spectral images of areas of the hybrid natural dental hard tissue/dental composite interface, but also to correlate the microstructure with molecular chemistry at the scale of a few microns [11,14].

Visualization of the interface features between dental restorative composite and natural tissue (dentin) plays an important role for the development of biomimetic approaches to dental restoration and is a subject of active study [4,19–21]. Thus, the importance of determining the surface quality and the conditions under which the type of chemical bond is formed, depending on the pre-treatment conditions of the dental tissue, has been repeatedly noted [11,19,22–25]. Both diamond drills (diamond turbines) and laser irradiation are used in the phase of dental restoration for the layer-by-layer removal of tissue, which in turn can also lead to undesirable effects, including an influence on the chemical and phase composition of dental tissue [24–29].

It should be noted that an analysis of the fine structural features of the dental tissue in the area of contact with restorative materials depending on the cavity preparation method used in the tooth has not been performed using spectral imaging. The aim of our work was therefore to investigate the effect of the medical dental laser and diamond drill on dentin tissue using spectral imaging and multivariate analysis of synchrotron FTIR microspectroscopy data.

2. Objects and Methods of Research

Intact third molars were used for the experiment. Human molar specimens were removed from donors (men and women aged 20–25 years) for orthodontic reasons.

All participants in the study were systemically healthy and had no unhealthy habits, as confirmed by their medical records. Dental samples had no cavities or erosions (ICDAS 0).

All donors provided their written consent for participation. The Ethics Committee of Voronezh State University affirmed the performed examination (Permission no. 001.017-2019, 21 December 2019).

After extraction, the teeth were placed in individual vials containing 0.9% physiological solution and 0.002% sodium azide and stored at 4 °C.

Before the experiments, the teeth were rinsed in running distilled water and cleaned of deposits on their surfaces for 10 min using a stiff brush. The samples were then dried with dry air using a compressor.

The collected tooth samples ($N = 20$) were randomly divided into two groups. The first group of samples was prepared by a diamond cylindrical drill with a turbine handpiece. A restorative cavity in the tooth enamel was formed at a speed of 4000 revolutions per minute and a water-jet cooling mode. When the dentin was reached, the preparation was carried out in stages with finishing of the cavity walls at low rotational speeds.

The Er:YAG pulsed laser (2940 nm, 75–500 μ s, 10–50 Hz) was used to generate a restorative cavity in the second group of specimens. The hard tissue was prepared with different laser powers: $P_e = 8$ W for enamel and $P_d = 4$ W for dentin.

The formed restorative cavity had a depth of ~6 mm and a diameter of ~4 mm, and was rinsed with distilled water and dried with an airflow from a compressor. In order to ensure micro-mechanical bonding to the adhesive as well as to remove the lubricated hard tissue layer according to the instructions of the manufacturer of the commercial bonding system, the cavity walls in the enamel were selectively treated with a 38% orthophosphoric acid-based gel for 30 s.

A commercial system was used for luting of the compomer, including dentin conditioner, bioprimer, BisGMA-based universal adhesive [19,30,31] and DyractXP dental material [32]. As demonstrated in previous studies [11,14], this system allows for the gentle removal of lubricated dentin, affects dentin proteins with a complex of amino acids incorporated into the bioprimer and increases the penetration ability of the universal adhesive containing the composite components [33].

After forming a cavity in the area of the chewing surface of the tooth enamel of each specimen using microbrushes, the inner walls and the bottom of the cavity formed in the upper part of the dentin were treated with 0.1 mL of bio-primer for 30 s. After treating the cavity, bioprimer was distributed on the surface of the cavity by air flow from a compressor for 10 s. After enduring for 20 s, BisGMA adhesive was applied to the prepared cavity and distributed on the surface of the cavity by the air stream from the compressor for 10 s. The adhesive was then photopolymerised for 5 s.

In the next step, DyractXP light-curing composite was applied to the internal surface of the cavity and photopolymerised following the manufacturer's instructions.

Afterwards, using a water-cooled diamond blade, thin slices were obtained from each sample and fixed on a glass substrate using acrylate adhesive. All samples were then gently polished using a diamond abrasive according to our tried and tested technique [14].

The synchrotron FTIR microspectroscopy measurements and spectral imaging of the teeth slices in macro-ATR-FTIR mapping mode were performed at the IRM beamline at Australian synchrotron. Using an in-house developed macro-ATR-FTIR device equipped with a 250-mm-diameter facet germanium (Ge) ATR crystal ($n_{\text{Ge}} = 4.0$), and a $20\times$ IR objective. The unique combination of the high refractive index property of the Ge ATR crystal and the high NA objective used in this device, when coupled to the IR-synchrotron beam, allows for surface characterization of the teeth slices to be performed at a high resolution without scattering artefacts. All the synchrotron FTIR spectra were recorded within a spectral range of 3800–700 cm^{-1} using 4- cm^{-1} spectral resolution. Blackman-Harris 3-Term apodization, Mertz phase correction, and a zero-filling factor of 2 were set as default acquisition parameters using OPUS 7.2 software suite (Bruker Optik, Mannheim, Germany).

Spectral data processing, averaging, maximum positioning, integral area values and decomposition into components was performed using OPUS 7.5 software suite (Bruker Optik) and Origin software.

Preliminary processing of the spectral data allowed for the removal of noise, increased the accuracy of chemometric analysis at the next stage and improved data interpretation of the multicomponent analysis.

The employed methods of preliminary processing included correction of the baseline, normalization and noise cancellation with smoothing according to the Savitzky–Golay

technique. The used baseline correction technique was obtained from the instrument of baseline correction provided by OPUS Bruker FTIR Software. All the spectra were smoothed (17 points), the baseline was corrected using a concave rubberband correction (10 iterations and 64 baseline points), and the spectra were normalized using vector normalization. The Savitzky–Golay smoothing parameter was the fourth degree of polynomial, second-order derivative, and 67 smoothing points. To make the optimization, the baseline corrected raw data within the spectral range of 3800–700 cm^{-1} wavenumbers were compared with the baseline corrected spectral data.

Multivariate data analysis to extract synthetic information and perform spectral imaging was carried out using hierarchical cluster analysis (HCA) and principal component analysis (PCA) sequentially.

In our work, the ATR-FTIR maps were evaluated using hierarchical cluster analysis (HCA). HCA permits the identification of regions within a sample structure based on their spectral response. Regions where the points display similar spectral responses demonstrate minimal intra-cluster spectral differences, while those with different spectral responses show maximal inter-cluster differences [11,13,22,34]. As the major vibrations characterizing the investigated materials are within the 1800–950 cm^{-1} range of the FTIR spectrum, second derivative and vector normalization were applied to this range to process raw spectral data for HCA. The spectra were smoothed over 17 points.

The optimal clustering algorithm was experimentally determined using Euclidean distance as the measure between clusters. Ward's method was used for clustering and construction of heterogeneity dendrograms. This method generates multiple partitions of the original image and considers all cluster (similar spectra) combinations using analysis of variance to assess the distance between clusters [35]. The number of clusters was determined based on technical data and a heterogeneity dendrogram. HCA was performed using OPUS v.7.5 software (Bruker Optik GmbH, Ettlingen, Germany).

Principal component analysis was used in the second stage of imaging to analyze the spectral dataset and identify correlations and similarities between the FTIR spectral response characteristic of particular clusters [11]. PCA was applied to the full range of FTIR spectra and performed using the first derivatives of the spectra. PCA was implemented in MATLAB environment (R2013b, Mathworks, Natick, MA, USA).

Preliminary consideration of the obtained experimental results demonstrated that the specimens within specific sampling (of the first or second type) showed similar characteristics: IR- and Raman spectra involved absolutely one and the same set of vibrational modes of the same type, specifying certain molecular bonds; clusterization revealed one and the same set of specific regions, typical images, and calculation data (see the Supplementary File). Results differed insignificantly between the samples within one sampling, and this was due to the individual local features of the hard tissue or the material. Taking into account this fact we present in our work the images as well as the spectral and calculated data typical for certain types of samples.

3. Results Obtained and Discussion

Typical optical slit images for the two types of samples we obtained are shown in Figure 1a,b.

It can be clearly seen that the reflected light images obtained using an optical microscope do not show any visual differences in the prepared hard tissue at the dentin/adhesive/composite interface. At the same time, the image analysis (Figure 1) shows that the macro- and micro-relief of the interface depends on the type of preparation. When the Er:YAG pulsed laser is used, as a result of rectilinear propagation of the laser beam, the shape of the cavity wall relief is close to rectilinear and is homogeneous. In the case of using a diamond cylindrical drill with a turbine handpiece for restorative cavity preparations, the macro-relief is determined by the shape and size of the bur and the micro-relief by the size of diamond grains on its surface. It should be noted that in the case of diamond cylindrical drills, the presence of microparticles of dental tissue is observed in the area of the interface (Figure 1b). The appearance of these particles

at the interface is due to the process of drilling with a diamond drill (drilling), as well as the subsequent preparation of dentin tissues. The presence of heterogeneous particles of different sizes depends on the surface profile of the diamond cylindrical bur and corresponds to the characteristic pattern of dentin preparation by drilling [36,37]. Neither the color contrast of the images, nor the permeability of the dental hard tissue, nor do the micro-relief studies, provide an indication of the condition of the hybrid layer (Figure 1c,d) formed during restorations. Spectral imaging [11,14,17,38,39] helps to obtain meaningful information about the chemical state in the interface area. For the samples we obtained using the synchrotron FTIR microspectroscopy technique, mapping in the interface region with a spatial resolution of ~ 500 nm was performed. Each point of the spectral map is a FTIR spectrum collected from a surface area of ~ 1 μm /pixel in diameter, which is given by the chosen microscope aperture.

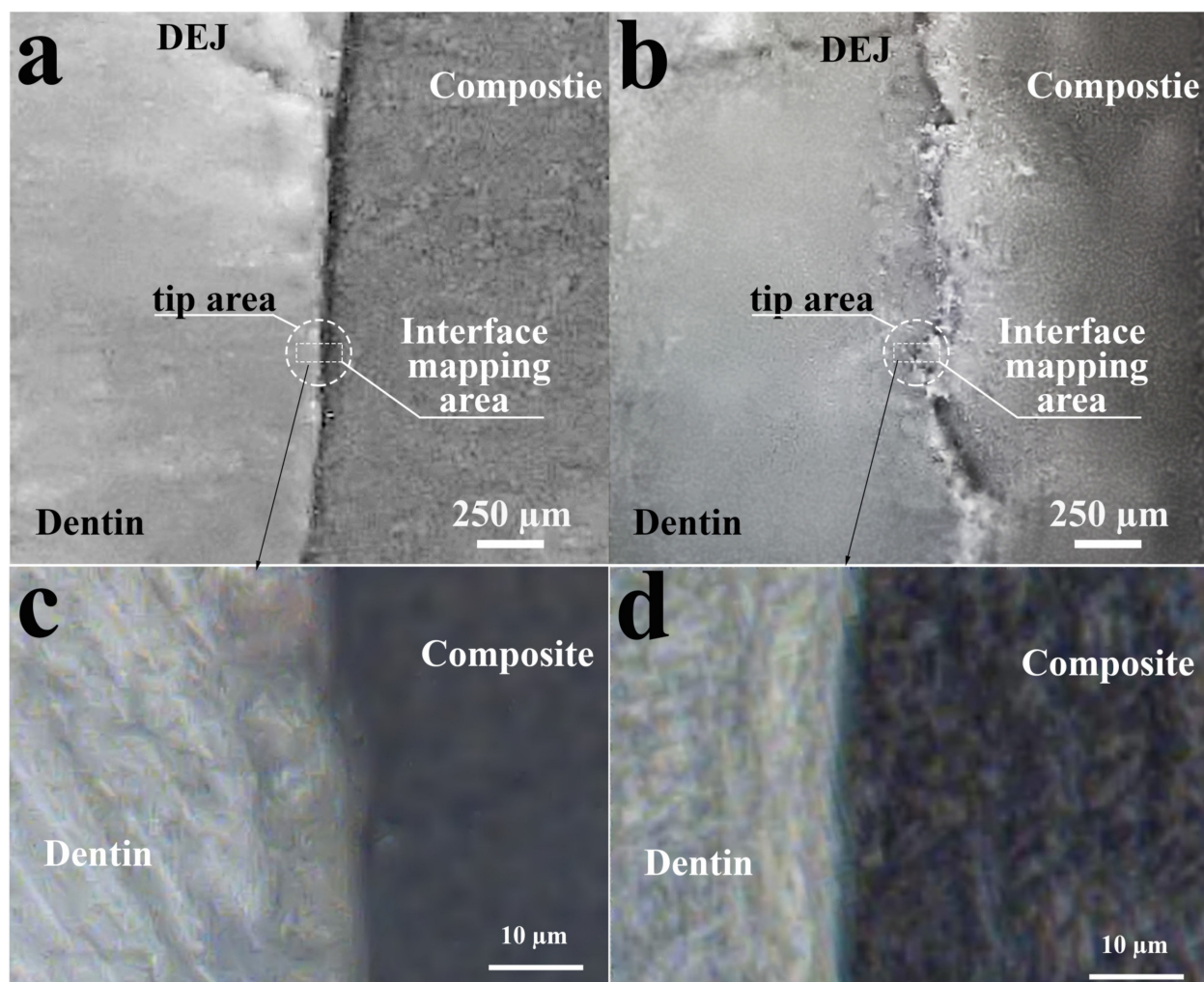


Figure 1. Optical resurfacing of the dental composite/dental tissue interface with different cavity wall formation techniques: (a) using an Er:YAG pulsed laser; (b) using a diamond cylindrical drill with a turbine handpiece; (c) interface mapping area 44×60 μm from interface prepared by Er:YAG pulsed laser; and (d) interface mapping area 44×60 μm from interface prepared by diamond cylindrical drill with a turbine handpiece.

Our previous works, as well as a number of similar publications, have demonstrated a technique of chemical imaging from the analyzed region where the intensity of the chemical/molecular group distribution is displayed using color-coding [10,11,14,16–18]. However, such images, although they reveal chemical distributions, do not always reveal the features of the mechanisms affecting molecular differentiation. Therefore, mathematical processing of the

obtained spectral map using multidimensional analysis methods is performed. This procedure makes it possible not only to systematize the array of spectra collected as FTIR images [14,40,41] but also to reveal the relationships between them. Mathematical analysis makes it possible to highlight information that may have been missed when studying the interface boundaries of biological samples which, by their nature, contain heterogeneous molecular compounds [42].

Figure 2a,b shows the typical results of spectral mapping of the interface regions in the cases of Er:YAG pulsed laser and diamond cylindrical drill with a turbine handpiece after a hierarchical cluster analysis (HCA) of the dataset. Additional HCA images of samples with different cavity wall forming methods are presented in the Supplementary File.

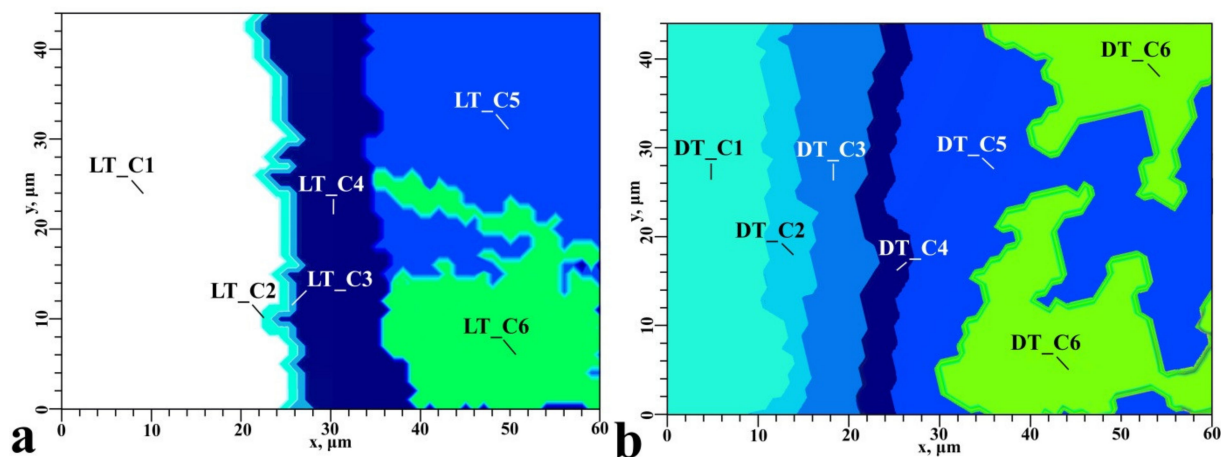


Figure 2. HCA in the area of dental composite/dental tissue interfaces with different cavity wall forming methods: (a) using an Er:YAG pulsed laser; and (b) using a diamond cylindrical drill with a turbine handpiece.

Initially, we tested four linkage rules (Ward's method, single, complete, and centroid linkages) with the same dataset. Based on visual inspection (evenly distributed clusters) and the cophenetic correlation coefficient which measures how faithfully a dendrogram preserves the pairwise distances between the original unmodeled data points and therefore helps one to determine how well the dendrogram preserved the structure of the original dataset, we have chosen Ward's method.

In contrast to optical microscopy (Figure 1c,d) the HCA results (Figure 2a,b) give an unambiguous image of the shape and boundaries of specific chemical zones in the analyzed area. The analysis of the HCA images (Figure 2a,b) shows that the boundaries between adjacent clusters in both types of samples have a distinctly straight shape, which correlates with the optical image of the interface boundary (Figure 1a,b). At the same time, the lateral location of the identified clusters allows for the characteristic areas in the interface area, and in particular in the zone of pre-treated dental hard tissue (Figure 2a,b), to be zoned. Six different clusters (LT_C1-LT_C6 and DT_C1-DT_C6, respectively) are shown in the interface mapping of $44 \times 60 \mu\text{m}$ in the area of Figure 1a,b, both for tissue prepared with an Er:YAG pulsed laser and with a diamond cylindrical drill with a turbine handpiece (Figure 2a,b). Interestingly, for the commercial material shown in the HCA images (Figure 2a,b), the localization and shape of the clusters are similar. At the same time, a linear spatial delineation of the clusters is observed in the dentin area represented in the HCA images of the interfaces on the left (Figure 2a,b). Given that the hybrid interface was formed using the same materials and under the same conditions, the HCA results suggest that the shape and size of the clusters in the same spatial region are dependent on the type of instrument used to prepare the dental tissue.

The analysis of averaged FTIR spectra of the clusters made it possible to determine the correspondence between the molecular composition of each zone in the HCA maps for both types of samples. For this purpose, at least 30 spectra were selected from each spatial

region, followed by smoothing, baseline correction, vector normalization and averaging procedures. The averaged spectra obtained in this way for each cluster of samples of both types are shown in Figure 3. FTIR spectra are presented without normalization for convenience of their comparison and visualization of low-intensive spectral features characteristic for a certain type of sample. In the Supplementary File, the averaged FTIR spectra for each cluster are presented with an error bar (standard deviation).

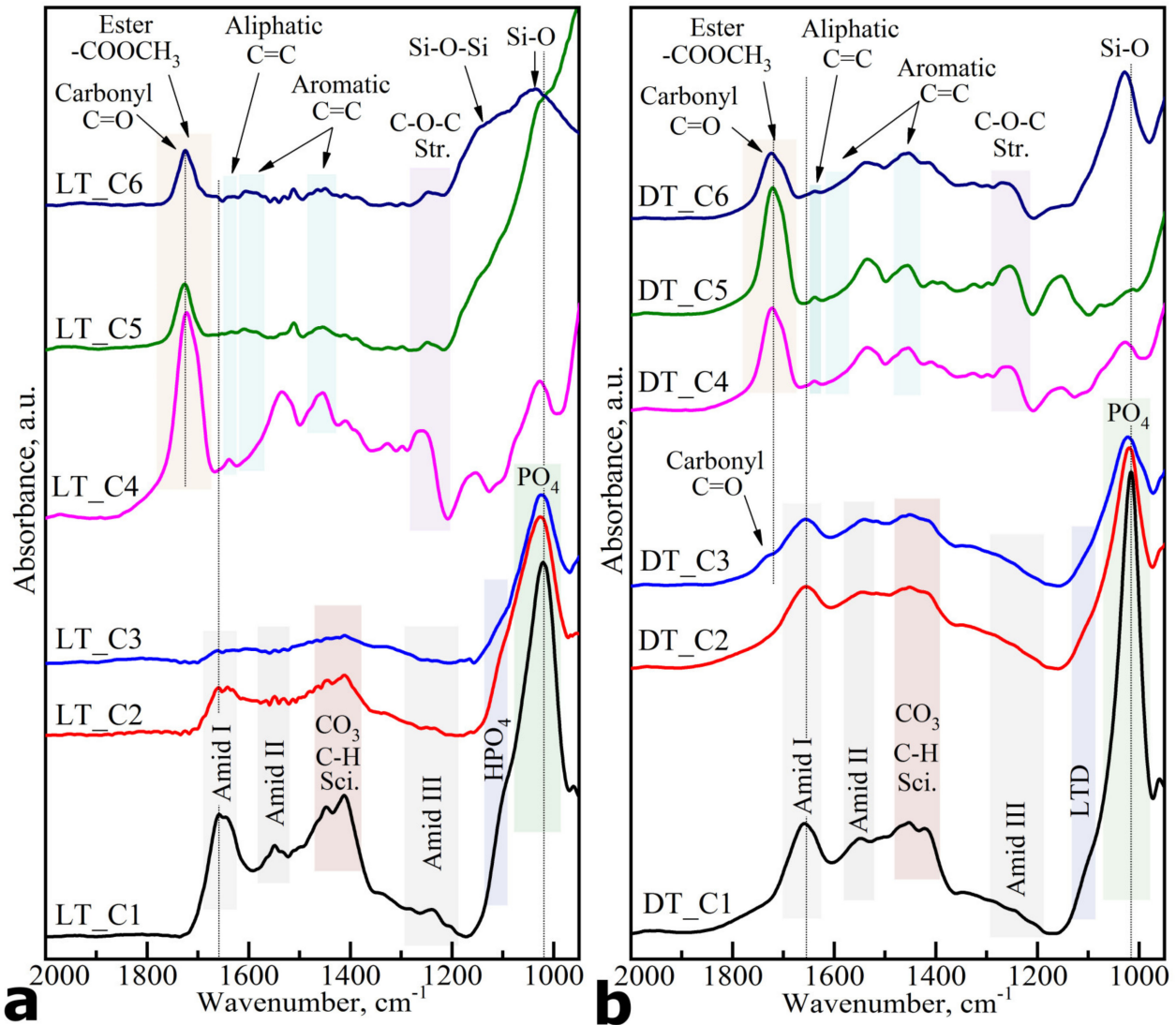


Figure 3. Averaged FTIR spectra of clusters from the interface region with different methods of cavity wall formation in the sample: (a) using Er:YAG pulsed laser; and (b) using a diamond cylindrical drill with a turbine handpiece.

In addition, Figure 4 shows the spectra of the commercial materials used during restorative cavity preparations: BisGMA adhesive [19,30], DyractXP light-curing composite [32] and bioprimer [22].

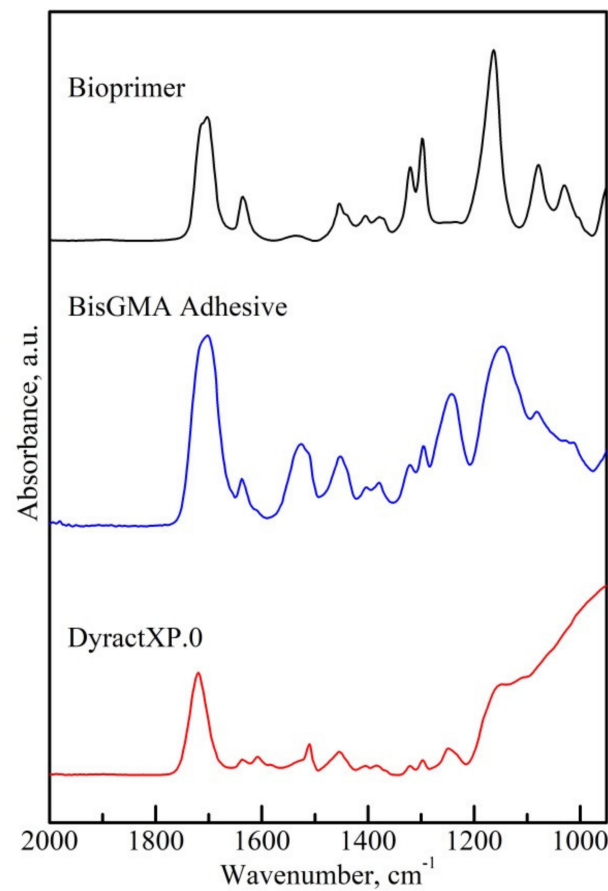


Figure 4. FTIR spectra of the materials used for restorative cavity preparations: BisGMA adhesive, DyractXP light-curing composite and bio-primer.

The analysis of the experimental spectra was performed using known data from the literature that analysed FTIR spectra of materials present in the interface zone [30,36,43–46], as well as laser-prepared dentin tissues [36,47–50]. The main vibrations and their characteristic functional groups and substances are marked in the spectra (see Figure 3a,b) and are also presented in Table 1.

Table 1. Active vibrations in the spectra of the dentin, BisGMA Adhesive, DyractXP commercial material. Intensity of vibration bands in the spectra.

Substance/ Material	Spectral Area, cm^{-1}	Functional (Molecular) Group	References
Dentin	1687–1662	LTD, $-\text{CO}-\text{NH}_2-$	[47–50]
	1644–1658	Amide I C=O stretching	[43,51–53]
	1636	LTD	[47–50]
	1605	LTD	[47–50]
	1549–1563	Amide II C–N stretching and N–H deformation modes, CNH	[43,53]
	1445–1456	Collagen C–H Scissoring, C–H bending	[43,52–55]
	1450 cm^{-1} 1415 and	$\nu_3 \text{CO}_3^{2-}$ substituted in B-type PO_3^{3-} and A-type OH and C–H Scissoring	[43,50,53–55]
	1330	LTD	[47–50]
	1320	C–H bending	[56]

Table 1. Cont.

Substance/ Material	Spectral Area, cm^{-1}	Functional (Molecular) Group	References
	1246 1234	amide III, N–H deformation C–N stretching	[43,52]
	1165	LTD	[47–50]
	1127–1145	HPO_4^{2-}	[57,58]
	1122	LTD	
	1100–1110	$\nu_3 \text{PO}_4$	[57]
	1090	Phosphate in dentin	[43]
	1061–1075	LTD Apatite $\nu_3 \text{PO}_4$, after laser ablation, pure HAP	[47–50,58]
	1030–1047	$\nu_3 \text{PO}_4$ apatite in dentin	[43,52,53]
	1027–1034	$\nu_3 \text{PO}_4$ Apatite PO_4 , after laser ablation, pure HAP	[52,55,58]
	1010–1020	$\nu_3 \text{PO}_4$ in poorly crystalline apatites	[58]
	964	$\nu_1 \text{PO}_4$	[58]
Conditioner + Amino acids booster	1718	C=O carbonyl group of AA	[59]
	1635	ν as, COO- vas(CN_3H^{+5})	[60]
	1460–1445	CH_2/CH_3	[60]
	1362	N-C α -H α , C β -C α -H α	[60]
	1226	NH_3^+	[60,61]
	1185	ρ, NH_3^+	[60]
Bioprimer	1703	C=O stretching	[62]
	1635	vas(CN_3H^{+5}) protein amino acid, arginine	[63,64]
	1454	$-\text{CH}_2$	[65]
	1320–1298	[$\nu(\text{C-O})$] stretch doublet $\delta(\text{CH})$	[62]
	1164	C–O–C, $\delta(\text{CH})$	[62]
	1078	$\nu(\text{CO})$	[65]
	1026	$\nu(\text{CC})$	[65]
BisGMA Adhesive	1721	C=O carbonyl	[19,66]
	1636	C=C Aliphatic C=C methacrylate groups	[66]
	1609	phenyl C=C	[66,67]
	1513	Aromatic C=C	[66]
	1452	$\text{CH}_2 \text{CH}_3$	[66,67]
	1402	$=\text{CH}_2$ deformation	[19]
	1320–1290	[$\nu(\text{C-O})$] stretch dublet	[19]
	1242	Aromatic C–O	[19]

Table 1. Cont.

Substance/ Material	Spectral Area, cm^{-1}	Functional (Molecular) Group	References
DyractXP commercial material	1700–1740	Ester groups $-\text{COOCH}_3$ attached to the methacrylate	[19,68]
	1636	C=C stretching vibration of the methacrylate group	[68,69]
	1608	C=C in an aromatic ring	[68,69]
	1511	N–H deformation stretching of urethane dimethacrylate (UDMA)	[68,69]
	1454	C–H in constituent monomers	[68]
	1297	symmetric stretching of –O in monomers, Si–O stretching	[68]
	1233	C–O–C stretching	[19,69]
	1150	C–O–C stretching	[19,69]
	1040–1060	Si–O from SiO_2 -containing fillers	[68,70]

The analysis of FTIR spectroscopy results and their comparison with the literature shows that for natural dentin, the most intense spectra are the characteristic vibrations of the inorganic component, and in particular the phosphate and carbonate groups involved in its composition. At the same time, structural transformations in the hard tissue may be traced through changes occurring in the form of the spectral profile of a band localized around $1000\text{--}1090\text{ cm}^{-1}$ and consisting of a number of overlapping modes associated with phosphate groups $-\text{PO}_4^{3-}$ [22,43,46,71]. The presence of variations in the fine structure of this spectral profile at different points of the analyzed region (clusters) is a consequence of the differentiation of the chemical composition. It is due to the formation of calcium phosphates with different stoichiometry, acidic phosphates (containing HPO_4^{2-} ion) [22,46,57,58], as well as the exposure of the hard tissue to the laser [47–50] or diamond drill. The vibrational modes associated with the presence of carbonate anion CO_3^{2-} in dentin correspond to stretching ν_3 and bending ν_4 vibrations located in the IR spectra between $1415\text{--}1450\text{ cm}^{-1}$ [43,50,53–55].

At the same time, next to the main phosphate band, Si–O bond oscillations of silica $1040\text{--}1090$, a filler for various commercial dental restorative systems/composites [68,70] can be observed.

As for the response from the organic component of dental hard tissue in FTIR spectra, the main modes associated with it are the absorption bands of amide groups (Amid I, Amid II, Amid III) belonging to proteins that are the parts of dentin collagen. The bands in the region of $1740\text{--}1710\text{ cm}^{-1}$ refer to vibrations of the ester group ($-\text{COOCH}_3$), which form part of BisGMA adhesive and DyractXP dental material [19,22,30–32,69]. In addition, the vibrations of N–H, C=O, COO– and CH molecular groups, which are part of the bioprimer used in dental restorations, are located in the region of $1690\text{--}1610\text{ cm}^{-1}$ and $1430\text{--}1370\text{ cm}^{-1}$ [22,30,31].

Based on the analysis of the FTIR spectroscopy data (Figure 3a,b), we identified the molecular composition of each cluster. For both types of samples, the clusters (LT_C1, LT_C2, LT_C3 and DT_C1, DT_C2, DT_C3) are located on the left side of the HCA spectral image (Figure 2a,b) and they correlate with the laser- or diamond cylindrical drill-prepared dental tissue. For the samples pretreated with the dental laser, the FTIR spectrum of the LT_C1 cluster is characteristic of natural dentin (Figure 3a). The main observed changes during the laser treatment of dentin occur in the region of phosphate band $1150\text{--}960\text{ cm}^{-1}$ [22,43,52,53]. The observed changes in the spectra of LT_C2 and LT_C3 clusters as compared to LT_C1 are associated with the appearance of a zone of demineralized/deorganized dentin resulting from the use of a dental laser for the preparation of dental tissue [48–50]. In contrast to the LT_C1 cluster, in the LT_C2 region located near the interface, the intensity of amide and CO_3^{2-} -absorption modes of the organic dentin component (collagen, proteins) decreases. This is typical for dentin layers pretreated with a low-power laser [48–50]. As LT_C2 is farther away from the interface than LT_C3, laser

irradiation was correspondingly less effective in this area. At the same time, the spectral composition of the LT_C3 cluster indicates that this region corresponds to dentin tissue that has been exposed to intense laser radiation [48,49]. The detected spectral changes indicate that the preparation of tissue with dental laser treatment may significantly alter the organic components of dentin, which may affect dentin adhesion [48,50,72]. Note that the mineral (phosphate) spectral band is characteristic of laser-treated dentin (LTD) tissue, which coincides with the known literature data for laser radiation of a similar strength [48,49]. Specific spectral features of the LT_C4 cluster indicate that the main component contained in this area is a BisGMA adhesive, whereas the LT_C5 and LT_C6 clusters include the components of commercially available restorative material [19,68].

As for the samples prepared with diamond bur, a gradient change in phase composition from the interface to the interior of the hard tissue from cluster DT_C3 to cluster DT_C1 is clearly visible (Figure 2b). Near the interface in dentin tissue, a decrease in the proportion of the crystalline inorganic component ($1000\text{--}1090\text{ cm}^{-1}$) is seen, the amplitude of its vibrations is at the level of the organic component ($1600\text{--}1700\text{ cm}^{-1}$) of DT_C3 (Figure 3b). The width of the phosphate band ($1000\text{--}1090\text{ cm}^{-1}$) of the DT_C3 cluster average spectrum is increased, the well-defined phosphate peak at 960 cm^{-1} shifts towards low frequencies, and the spectral profile itself becomes similar to the spectrum of amorphous calcium phosphate [46,50]. As one moves away from the interface, the intensity of the phosphate and carbonate bands increases, which can be observed in the spectra of DT_C2 and DT_C1 clusters. However, it should be noted that the spectral composition of the DT_C1 cluster does not correspond to the spectral composition of intact dentin, which was observed in the LT_C1 laser-prepared samples (Figure 3a,b). A comparison of the spectrum of DT_C1 cluster with the data from the reference list [22,43,46,71], as well as with that one of LT_C1 cluster (coinciding with the spectrum of intact dentin) shows the changes in the shape of the spectral profile in the high-intensive band attributed to the phosphate groups in the range of $1127\text{--}1145\text{ cm}^{-1}$, $1061\text{--}1075\text{ cm}^{-1}$, $1030\text{--}1047\text{ cm}^{-1}$. As it was shown in [36,46,71], such rebuilding corresponds to the structural changes in the apatite lattice and indicates destructive changes proceeding in the dentin. Rebuilding of the spectral profile of the phosphate band for the spectrum of DT_C1 cluster is connected with thermal heating of this area in dentin within the boundary region of the hybrid interface since this group of samples was prepared with the use of a microturbine handpiece and diamond bur [37]. At the same time, this indicates the greater depth of exposure of the dental tissue to the diamond bur than to the laser. In addition, a redistribution of the relative intensities of the Amid I, Amid II, Amid III bands as well as of the calcium phosphate-related PO_4 groups is observed in the DT_C1 averaged spectrum. Changes in the spectra in the amide vibrational bands may be attributed to changes in the secondary structure of the proteins and in the phosphate mode due to the occurrence of additional phases of weak calcium phosphates [47–50].

The cluster analysis also shows that preparation of dentin tissue with a diamond cylindrical bur results in the ingress of dentin microparticles, which were not removed after treatment because of the morphological features of the tissue [36,37,73,74]. It should be noted that the spectrum of DT_C3 shows the presence of molecular vibrational bands correlated with both the prepared dentin and the BisGMA adhesive (Figure 3b). The spectrum of the DT_C3 cluster, arranged in the area of the hybrid interface, involves vibrations as characteristic for dentin as those associated with adhesive components. A feature (low-intensive “shoulder”) in the range of $1720\text{--}1740\text{ cm}^{-1}$ marked in Figure 3b is attributed to the vibrations of the C=O carbonyl group in BisGMA adhesive. The low intensity of these vibrations is due to the narrow spatial area in dentin where the adhesive has penetrated and thus the latter is characterized by low content in this region (Figure 3b). At the same time, in the DT_C4 spectrum only the bands from BisGMA adhesive are present.

A comparison of the HCA images and the averaged spectra of the clusters shows that, in terms of molecular composition and its spatial distribution, clusters LT_C4 and DT_C3 and DT_C4 are associated with the formation of a $\sim 9\text{ }\mu\text{m}$ hybrid layer, where the components of BisGMA adhesive and bioprimer are present. On the right side of the spectral HCA images for both types of samples there are clusters (DT_C5, DT_C6 and

LT_C5, LT_C6), where spectral modes are detected (their contribution is fixed) from the components of the restorative composite, meaning that the filling is composed of SiO₂ silica, bio-primer and adhesive. The SiO₂ clusters of the filler, however, have a shape specific to silica aggregate particles, while the other clusters have an extended layered shape, that we have observed previously in our work related to the study of enamel restoration processes [11]. The existing local variation in the composition of the clusters attributed to the restorative material is related to non-homogeneous mixing of the chemical components used.

A multivariate principal component analysis (PCA) [11,75] was performed to compare the spectral composition of clusters in dentin where cavity walls were prepared with an Er:YAG pulsed laser and a diamond cylindrical drill with a turbine handpiece. This automated technique allowed us to differentiate chemicals in clusters belonging to the same type of spectral regions from the dentin preparation area. The results of PCA (scores (Figure 5) and loadings (Figure 6), allowed us to identify similarities and differences between them at the molecular level, as well as to differentiate (determine the largest difference) the changes occurring with a submicron spatial resolution.

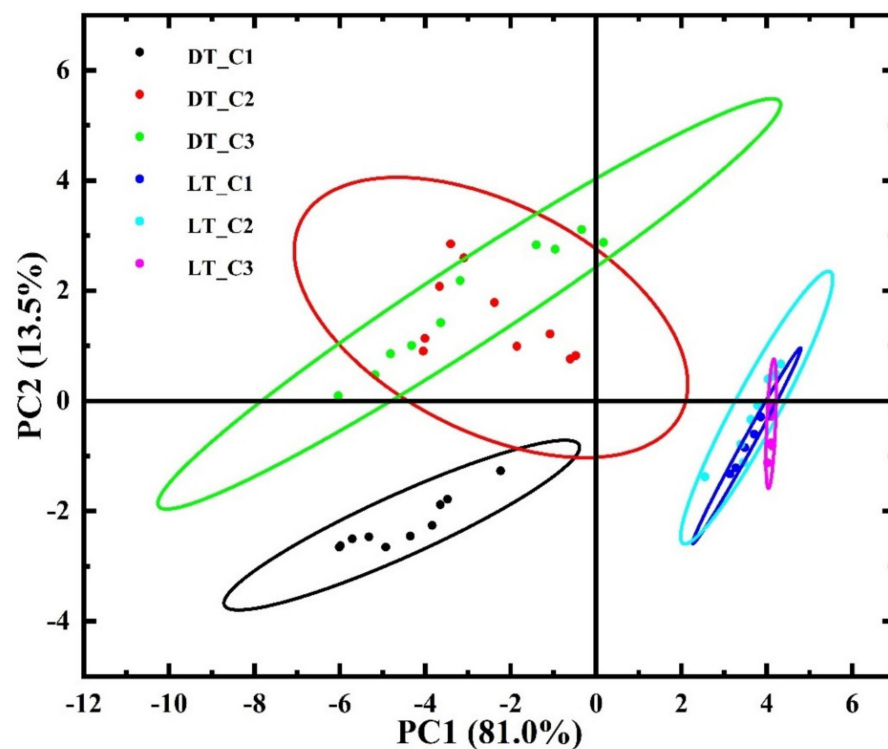


Figure 5. PCA values for clusters of dentin cavities prepared with an Er:YAG pulsed laser (LT_C1, LT_C2, LT_C3) and with a diamond cylindrical drill with a turbine handpiece (DT_C1, DT_C2, DT_C3).

Figure 5 visualises the results of PCA performed on HCA clusters (Figure 3a,b) from the dentin area prepared using an Er:YAG pulsed laser and employing a diamond cylindrical drill with a turbine handpiece. Each cluster is represented as an ellipse in the PCA picture. Additionally, the wave number loadings for the main components PC1 and PC2 are shown in Figure 6. It can be clearly seen that the PCA plots (Figure 4) show a clear separation between the clusters of laser-pre-treated and diamond cylindrical drill-treated samples, which once again confirms the different effects on the native tissue of its preparation methods. The PCA results show that the main differences between the clusters of the samples of both types can be explained by the components PC1 (81.0%) and PC2 (13.5%) (Figure 6). At the same time, ellipses DT_C2 and DT_C3, which correspond to dentin clusters in samples prepared with a diamond cylindrical drill with a turbine handpiece, as well as ellipses LT_C1 to LT_C3, which correspond to clusters in tissue pretreated with the

Er:YAG pulsed laser, are clustered and overlapped (Figure 5). This indicates similarity in the spectra (molecular properties) at these sites of pre-treated dental tissue. It is clear from the analysis of the score curves that the ellipses LT_C1–LT_C3 extend along PC1, while DT_C2 and DT_C3 extend along PC2 for the most part. This means that the differentiation in the dental tissue of these clusters is due to the indicated components and hence the corresponding loadings.

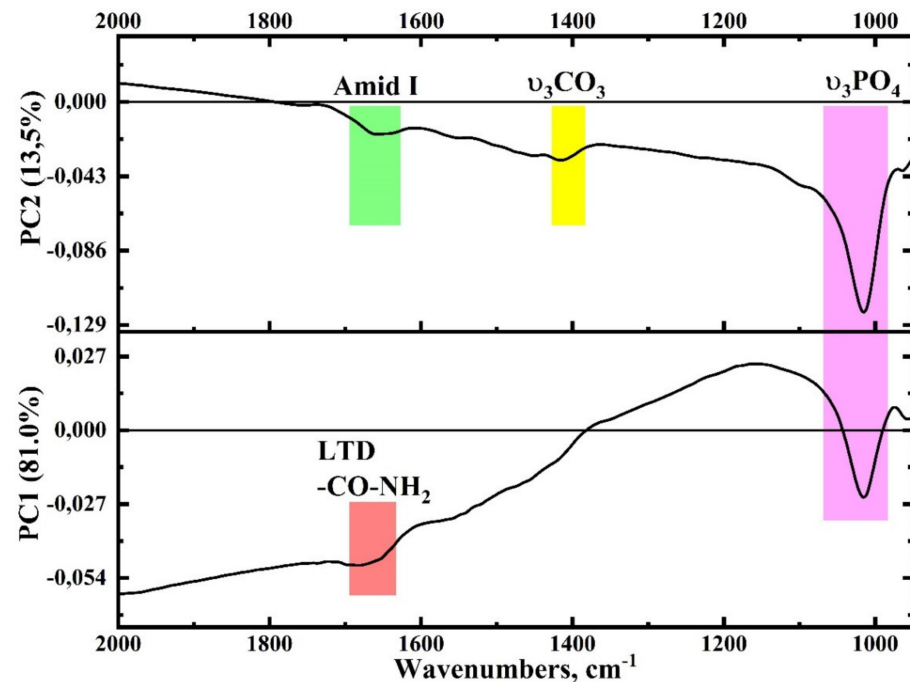


Figure 6. PCA loadings for PC1 and PC2 components.

The loadings plots shown in Figure 6 visualize a set of maxima/minima that contribute mainly to the observed differences between the interface areas of the two sample types and can be correlated with the vibrational groups present in the infrared spectra (Figure 3a,b) (Table 1). For convenience, such functional molecular groups (signatures) are color-coded in the load plots (Figure 6). The interpretation of these bands is based on known data in the literature [30,36,43–46,68,70,71]. The analysis shows that the differentiation of pre-treated dental tissue (dentin) using two different techniques can be performed using a set of FTIR modes including phosphate and carbonate bands as well as the vibrations associated with changes in the secondary dentin structure (LTD, $-\text{CO}-\text{NH}_2$ -) and Amid I band.

We would like to note that the use of univariate methods of analysis does not allow for the differences in the interphase structure to be revealed between the sound dental tissue and tissue pre-treated with the use of laser irradiation and the microturbine diamond drill handpiece. As this was noted in a series of works, the fact can be related to the limitations of univariate approaches in revealing the spectral changes. These problems were solved with the use of multivariate techniques, in particular by employing clusterization of the hyperspectral data array collected in FTIR maps and also by using the PCA method. Using methods of multi-component analysis (clusterization and PCA) made it possible to efficiently classify a great number of multi-component FTIR spectra and identify spatial areas in the regions of dental tissue pre-treated by different methods while approaching the interface. By applying clusterization techniques and PCA we can detect and display visually indiscernible and quite often even spectroscopically insignificant changes in the chemical structure proceeding in the hard dental tissue (dentin) depending on the method used for its pre-treatment. We are also able to classify and differentiate the revealed features at the sub-micrometer level with a high spatial resolution.

4. Conclusions

In summary, the combination of FTIR spectral imaging and subsequent multivariate analysis (HCA and PCA) allows for the clear detection of visually indistinguishable structural changes occurring in the dental hard tissue (dentin), depending on the pre-treatment method used, as well as the classification and differentiation of the identified features at a submicron level, with a high spatial resolution.

The detectable spectral transformations indicate that dental cavity preparation with a dental laser leads to significant changes in the organic components of dentin, which can affect adhesion. The use of a diamond cylindrical drill with a turbine handpiece demonstrates a larger extent of the altered hard tissue than the use of a dental laser for dental cavity preparation. The observed redistribution of the phase composition of inorganic component in the tissue is due to the occurrence of additional phases of weak calcium phosphates, and changes in the organic component to the transformation of the secondary protein structure.

Active use of the proposed integrated approach in the future will clarify its areas of applicability to the analysis of biological tissues and the pathologies in them, which will help to choose the best personalized approach for patients in clinical settings.

Supplementary Materials: The following supporting information can be downloaded at: <https://www.mdpi.com/article/10.3390/photonics10080881/s1>, Hyperspectral Mapping Steps in the Dental Office Area with Topological Reference; HCA images in the area of dental composite/dental tissue interfaces with cavity wall formation in the sample by an Er:YAG pulsed laser; HCA images in the area of dental composite/dental tissue interfaces with cavity wall formation in the sample by diamond cylindrical drill with a turbine handpiece; The averaged spectra of clusters with the error deviation bar (standard deviation) from the interface region with cavity wall formation in the sample using Er:YAG pulsed laser; The averaged spectra of clusters with the error deviation bar (standard deviation) from the interface region with cavity wall formation in the sample using diamond cylindrical drill with a turbine handpiece.

Author Contributions: P.S.: Conceived and designed the experiments, analysed the data, performed the experiments, contributed reagents/materials/analysis tools, and wrote the manuscript. D.G.: Contributed reagents/materials/analysis tools, performed the experiments, analysed the data, prepared the figures and/or tables and wrote the manuscript. Y.I. and I.I.: Contributed reagents/materials/analysis tools. V.K., N.B., D.N., J.V. and S.K. performed the experiments. All authors have read and agreed to the published version of the manuscript.

Funding: This work was funded by a grant from the Russian Science Foundation, grant number 21-15-00026; The access to scientific equipment and methodology was provided under support of the Ministry of Science and Higher Education of Russia, Agreement N 075-15-2021-1351.

Institutional Review Board Statement: The study was conducted according to the guidelines of the Declaration of Helsinki and approved by the Ethics Committee of Voronezh State University (Permission no. 001.017-2019, 21 December 2019).

Informed Consent Statement: Informed consent was obtained from all subjects involved in the study.

Data Availability Statement: The data that support the findings of this study are available from the corresponding author upon reasonable request.

Acknowledgments: Part of this research was undertaken with The Infrared Microspectroscopy (IRM) beamline at the Australian Synchrotron.

Conflicts of Interest: The authors declare no conflict of interest.

References

1. Ahmedt-Aristizabal, D.; Armin, A.; Denman, S.; Fookes, C.; Petersson, L. Graph-Based Deep Learning for Medical Diagnosis and Analysis: Past, Present and Future. *Sensors* **2021**, *21*, 4758. [[CrossRef](#)] [[PubMed](#)]
2. Besnard, C.; Harper, R.A.; Moxham, T.E.J.; James, J.D.; Storm, M.; Salvati, E.; Landini, G.; Shelton, R.M.; Korsunsky, A.M. 3D Analysis of Enamel Demineralisation in Human Dental Caries Using High-Resolution, Large Field of View Synchrotron X-Ray Micro-Computed Tomography. *Mater. Today Commun.* **2021**, *27*, 102418. [[CrossRef](#)]

3. Kenesei, K.; Murali, K.; Czéh, Á.; Piella, J.; Puentes, V.; Madarász, E. Enhanced Detection with Spectral Imaging Fluorescence Microscopy Reveals Tissue- and Cell-Type-Specific Compartmentalization of Surface-Modified Polystyrene Nanoparticles. *J. Nanobiotechnol.* **2016**, *14*, 55. [[CrossRef](#)] [[PubMed](#)]
4. Besnard, C.; Marie, A.; Sasidharan, S.; Harper, R.A.; Shelton, R.M.; Landini, G.; Korsunsky, A.M. Synchrotron X-Ray Studies of the Structural and Functional Hierarchies in Mineralised Human Dental Enamel: A State-of-the-Art Review. *Dent. J.* **2023**, *11*, 98. [[CrossRef](#)]
5. Pullano, S.A.; Bianco, M.G.; Greco, M.; Mazzuca, D.; Nisticò, S.P.; Fiorillo, A.S. FT-IR Saliva Analysis for the Diagnosis of Psoriasis: A Pilot Study. *Biomed. Signal Process. Control* **2022**, *74*, 103525. [[CrossRef](#)]
6. Calzolari, A.; Pavan, B.; Curtarolo, S.; Buongiorno Nardelli, M.; Fornari, M. Vibrational Spectral Fingerprinting for Chemical Recognition of Biominerals. *ChemPhysChem* **2020**, *21*, 770–778. [[CrossRef](#)]
7. Seredin, P.; Goloshchapov, D.; Kashkarov, V.; Emelyanova, A.; Buylov, N.; Ippolitov, Y.; Prutskij, T. Development of a Visualisation Approach for Analysing Incipient and Clinically Unrecorded Enamel Fissure Caries Using Laser-Induced Contrast Imaging, MicroRaman Spectroscopy and Biomimetic Composites: A Pilot Study. *J. Imaging* **2022**, *8*, 137. [[CrossRef](#)]
8. Vongsvivut, J.; Pérez-Guaita, D.; Wood, B.R.; Heraud, P.; Khambatta, K.; Hartnell, D.; Hackett, M.J.; Tobin, M.J. Synchrotron Macro ATR-FTIR Microspectroscopy for High-Resolution Chemical Mapping of Single Cells. *Analyst* **2019**, *144*, 3226–3238. [[CrossRef](#)]
9. Freitas, R.O.; Cemescu, A.; Engdahl, A.; Paulus, A.; Levandoski, J.E.; Martinsson, I.; Hebisch, E.; Sandt, C.; Gouras, G.K.; Prinz, C.N.; et al. Nano-Infrared Imaging of Primary Neurons. *Cells* **2021**, *10*, 2559. [[CrossRef](#)]
10. Babot-Marquillas, C.; Sánchez-Martín, M.-J.; Amigo, J.M.; Yousef, I.H.; Valido, I.; Boada, R.; Valiente, M. Tooth Whitening, Oxidation or Reduction? Study of Physicochemical Alterations in Bovine Enamel Using Synchrotron Based Micro-FTIR. *Dent. Mater.* **2022**, *38*, 670–679. [[CrossRef](#)]
11. Seredin, P.; Goloshchapov, D.; Kashkarov, V.; Khydyakov, Y.; Nesterov, D.; Ippolitov, I.; Ippolitov, Y.; Vongsvivut, J. Development of a Hybrid Biomimetic Enamel-Biocomposite Interface and a Study of Its Molecular Features Using Synchrotron Submicron ATR-FTIR Microspectroscopy and Multivariate Analysis Techniques. *Int. J. Mol. Sci.* **2022**, *23*, 11699. [[CrossRef](#)]
12. Zepeda-Zepeda, M.A.; Picquart, M.; Irigoyen-Camacho, M.E.; Mejía-Gózález, A.M. Diagnosis of Dental Fluorosis Using Micro-Raman Spectroscopy Applying a Principal Component-Linear Discriminant Analysis. *Int. J. Environ. Res. Public Health* **2021**, *18*, 10572. [[CrossRef](#)] [[PubMed](#)]
13. Seredin, P.; Goloshchapov, D.; Kashkarov, V.; Nesterov, D.; Ippolitov, Y.; Ippolitov, I.; Vongsvivut, J. Effect of Exo/Endogenous Prophylaxis Dentifrice/Drug and Cariogenic Conditions of Patient on Molecular Property of Dental Biofilm: Synchrotron FTIR Spectroscopic Study. *Pharmaceutics* **2022**, *14*, 1355. [[CrossRef](#)] [[PubMed](#)]
14. Seredin, P.; Goloshchapov, D.; Kashkarov, V.; Ippolitov, Y.; Ippolitov, I.; Vongsvivut, J. To the Question on the Use of Multivariate Analysis and 2D Visualisation of Synchrotron ATR-FTIR Chemical Imaging Spectral Data in the Diagnostics of Biomimetic Sound Dentin/Dental Composite Interface. *Diagnostics* **2021**, *11*, 1294. [[CrossRef](#)] [[PubMed](#)]
15. Seredin, P.; Goloshchapov, D.; Ippolitov, Y. Jitraporn Vongsvivut Spectroscopic Signature of the Pathological Processes of Carious Dentine Based on FTIR Investigations of the Oral Biological Fluids. *Biomed. Opt. Express BOE* **2019**, *10*, 4050–4058. [[CrossRef](#)]
16. Querido, W.; Falcon, J.M.; Kandel, S.; Pleshko, N. Vibrational Spectroscopy and Imaging: Applications for Tissue Engineering. *Analyst* **2017**, *142*, 4005–4017. [[CrossRef](#)]
17. Ye, Q.; Spencer, P. Analyses of Material-Tissue Interfaces by Fourier Transform Infrared, Raman Spectroscopy, and Chemometrics. In *Material-Tissue Interfacial Phenomena*; Elsevier: Amsterdam, The Netherlands, 2017; pp. 231–251. ISBN 978-0-08-100330-5.
18. Amarie, S.; Zaslansky, P.; Kajihara, Y.; Griesshaber, E.; Schmahl, W.W.; Keilmann, F. Nano-FTIR Chemical Mapping of Minerals in Biological Materials. *Beilstein J. Nanotechnol.* **2012**, *3*, 312–323. [[CrossRef](#)]
19. Delgado, A.H.; Young, A.M. Modelling ATR-FTIR Spectra of Dental Bonding Systems to Investigate Composition and Polymerisation Kinetics. *Materials* **2021**, *14*, 760. [[CrossRef](#)]
20. Betancourt, D.E.; Baldion, P.A.; Castellanos, J.E. Resin-Dentin Bonding Interface: Mechanisms of Degradation and Strategies for Stabilization of the Hybrid Layer. *Int. J. Biomater.* **2019**, *2019*, e5268342. [[CrossRef](#)]
21. Sato, T.; Takagaki, T.; Hatayama, T.; Nikaido, T.; Tagami, J. Update on Enamel Bonding Strategies. *Front. Dent. Med.* **2021**, *2*, 666379. [[CrossRef](#)]
22. Seredin, P.; Goloshchapov, D.; Ippolitov, Y.; Vongsvivut, J. Engineering of a Biomimetic Interface between a Native Dental Tissue and Restorative Composite and Its Study Using Synchrotron FTIR Microscopic Mapping. *Int. J. Mol. Sci.* **2021**, *22*, 6510. [[CrossRef](#)] [[PubMed](#)]
23. Perdigão, J. Current Perspectives on Dental Adhesion: (1) Dentin Adhesion—Not There Yet. *Jpn. Dent. Sci. Rev.* **2020**, *56*, 190–207. [[CrossRef](#)] [[PubMed](#)]
24. Kaptan, A.; Oznurhan, F. Effects of Er:YAG and Er,Cr:YSGG Laser Irradiation and Adhesive Systems on Microtensile Bond Strength of a Self-Adhering Composite. *Lasers Med. Sci.* **2023**, *38*, 41. [[CrossRef](#)] [[PubMed](#)]
25. Valinhos Piccioni, M.A.R.; Giroto, A.C.; Saad, J.R.C.; de Campos, E.A. Influence of Different Surface Protocols on Dentin Bond Strength Irradiated with Er,Cr:YSGG Laser. *Laser Dent. Sci.* **2019**, *3*, 43–51. [[CrossRef](#)]
26. Chowdhury, A.F.M.A.; Islam, R.; Alam, A.; Matsumoto, M.; Yamauti, M.; Carvalho, R.M.; Sano, H. Variable Smear Layer and Adhesive Application: The Pursuit of Clinical Relevance in Bond Strength Testing. *Int. J. Mol. Sci.* **2019**, *20*, 5381. [[CrossRef](#)]
27. Lagunov, V.L.; Rybachuk, M.; Itthagarun, A.; Walsh, L.J.; George, R. Modification of Dental Enamel, Dentin by an Ultra-Fast Femtosecond Laser Irradiation: A Systematic Review. *Opt. Laser Technol.* **2022**, *155*, 108439. [[CrossRef](#)]

28. Mahdisiar, F.; Mirzaei, A.; Fallah, A.; Gutknecht, N.; Akhoundan, S. Effect of Duration of Er,Cr:YSGG Laser Etching on Dentin Morphology: An in Vitro Study. *Lasers Dent. Sci.* **2018**, *2*, 213–219. [[CrossRef](#)]
29. Petrov, T.; Pecheva, E.; Walmsley, A.D.; Dimov, S. Femtosecond Laser Ablation of Dentin and Enamel for Fast and More Precise Dental Cavity Preparation. *Mater. Sci. Eng. C* **2018**, *90*, 433–438. [[CrossRef](#)]
30. Seredin, P.V.; Goloshchapov, D.L.; Prutskij, T.; Ippolitov, Y.A. Fabrication and Characterisation of Composites Materials Similar Optically and in Composition to Native Dental Tissues. *Results Phys.* **2017**, *7*, 1086–1094. [[CrossRef](#)]
31. Seredin, P.V.; Goloshchapov, D.L.; Nikitkov, K.A.; Kashkarov, V.M.; Ippolitov, Y.A.; Jitraporn (Pimm), V. Application of Synchrotronic IR-Microspectroscopy for Analysis of Integration of Biomimetic Composites with Native Dental Tissues. *Condens. Matter Interphases* **2019**, *21*, 262–277. [[CrossRef](#)]
32. Tekçe, N.; Tuncer, S.; Demirci, M.; Serim, M.E.; Baydemir, C. The Effect of Different Drinks on the Color Stability of Different Restorative Materials after One Month. *Restor. Dent. Endod.* **2015**, *40*, 255–261. [[CrossRef](#)] [[PubMed](#)]
33. Seredin, P.V.; Uspenskaya, O.A.; Goloshchapov, D.L.; Ippolitov, I.Y.; Vongsvivut, J.; Ippolitov, Y.A. Organic-Mineral Interaction between Biomimetic Materials and Hard Dental Tissues. *Sovrem. Tehnol. V Med.* **2020**, *12*, 43. [[CrossRef](#)] [[PubMed](#)]
34. Wang, Y.; Yao, X.; Parthasarathy, R. Characterization of Interfacial Chemistry of Adhesive/Dentin Bond Using FTIR Chemical Imaging with Univariate and Multivariate Data Processing. *J. Biomed. Mater. Res. A* **2009**, *91*, 251–262. [[CrossRef](#)]
35. Savić, D.; Joković, N.; Topisirović, L. Multivariate Statistical Methods for Discrimination of Lactobacilli Based on Their FTIR Spectra. *Dairy Sci. Technol.* **2008**, *88*, 273–290. [[CrossRef](#)]
36. Jegova, G.; Titorenkova, R.; Rashkova, M.; Mihailova, B. Raman and IR Reflection Micro-Spectroscopic Study of Er:YAG Laser Treated Permanent and Deciduous Human Teeth. *J. Raman Spectrosc.* **2013**, *44*, 1483–1490. [[CrossRef](#)]
37. Shamsudeen, S.M.; Thavarajah, R.; Joshua, E.; Rao, U.D.K.; Kannan, R. Evaluating and Comparing the Morphological and Histopathological Changes Induced by Erbium:Yttrium-Aluminum-Garnet Laser and Diamond Bur on Enamel, Dentin and Pulp Tissue. *J. Investig. Clin. Dent.* **2019**, *10*, e12475. [[CrossRef](#)] [[PubMed](#)]
38. Wang, Z.; Wang, K.; Xu, W.; Gong, X.; Zhang, F. Mapping the Mechanical Gradient of Human Dentin-Enamel-Junction at Different Intratooth Locations. *Dent. Mater.* **2018**, *34*, 376–388. [[CrossRef](#)] [[PubMed](#)]
39. Querido, W.; Kandel, S.; Pleshko, N. Applications of Vibrational Spectroscopy for Analysis of Connective Tissues. *Molecules* **2021**, *26*, 922. [[CrossRef](#)]
40. Kobrina, Y.; Rieppo, L.; Saarakkala, S.; Pulkkinen, H.J.; Tiitu, V.; Valonen, P.; Kiviranta, I.; Jurvelin, J.S.; Isaksson, H. Cluster Analysis of Infrared Spectra Can Differentiate Intact and Repaired Articular Cartilage. *Osteoarthr. Cartil.* **2013**, *21*, 462–469. [[CrossRef](#)]
41. Seredin, P.; Goloshchapov, D.; Kashkarov, V.; Khudyakov, Y.; Ippolitov, I.; Ippolitov, Y.; Vongsvivut, J. Biomimetic Nano-c-HAP Hybrid Layer Engineering and Determination of Mechanisms of Its Integration with Native Hard Dental Tissue. *Results Eng.* **2021**, *11*, 100266. [[CrossRef](#)]
42. Ogruc Ildiz, G.; Karadag, A.; Kaygisiz, E.; Fausto, R. PLS-DA Model for the Evaluation of Attention Deficit and Hyperactivity Disorder in Children and Adolescents through Blood Serum FTIR Spectra. *Molecules* **2021**, *26*, 3400. [[CrossRef](#)] [[PubMed](#)]
43. de Carvalho Almança Lopes, C.; Limirio, P.H.J.O.; Novais, V.R.; Dechichi, P. Fourier Transform Infrared Spectroscopy (FTIR) Application Chemical Characterization of Enamel, Dentin and Bone. *Appl. Spectrosc. Rev.* **2018**, *53*, 747–769. [[CrossRef](#)]
44. Reyes-Gasga, J.; Martínez-Piñeiro, E.L.; Rodríguez-Álvarez, G.; Tiznado-Orozco, G.E.; García-García, R.; Brès, E.F. XRD and FTIR Crystallinity Indices in Sound Human Tooth Enamel and Synthetic Hydroxyapatite. *Mater. Sci. Eng. C* **2013**, *33*, 4568–4574. [[CrossRef](#)] [[PubMed](#)]
45. Jeon, R.J.; Hellen, A.; Matvienko, A.; Mandelis, A.; Abrams, S.H.; Amaechi, B.T. In Vitro Detection and Quantification of Enamel and Root Caries Using Infrared Photothermal Radiometry and Modulated Luminescence. *J. Biomed. Opt.* **2008**, *13*, 034025. [[CrossRef](#)] [[PubMed](#)]
46. Rey, C.; Marsan, O.; Combes, C.; Drouet, C.; Grossin, D.; Sarda, S. Characterization of Calcium Phosphates Using Vibrational Spectroscopies. In *Advances in Calcium Phosphate Biomaterials*; Springer Series in Biomaterials Science and Engineering; Springer: Berlin/Heidelberg, Germany, 2014; pp. 229–266. ISBN 978-3-642-53979-4.
47. Bakry, A.S.; Sadr, A.; Takahashi, H.; Otsuki, M.; Tagami, J. Analysis of Er:YAG Lased Dentin Using Attenuated Total Reflectance Fourier Transform Infrared and X-Ray Diffraction Techniques. *Dent. Mater. J.* **2007**, *26*, 422–428. [[CrossRef](#)]
48. Zezell, D.M.; Benetti, C.; Veloso, M.N.; Castro, P.A.A.; Ana, P.A. FTIR Spectroscopy Revealing the Effects of Laser and Ionizing Radiation on Biological Hard Tissues. *J. Braz. Chem. Soc.* **2015**, *26*, 2571–2582. [[CrossRef](#)]
49. Le, Q.-T.; Bertrand, C.; Vilar, R. Structural Modifications Induced in Dentin by Femtosecond Laser. *J. Biomed. Opt.* **2016**, *21*, 125007. [[CrossRef](#)]
50. Le, Q.T.; Vilar, R.; Bertrand, C. Influence of External Cooling on the Femtosecond Laser Ablation of Dentin. *Lasers Med. Sci.* **2017**, *32*, 1943–1951. [[CrossRef](#)]
51. Sasaki, K.M.; Aoki, A.; Masuno, H.; Ichinose, S.; Yamada, S.; Ishikawa, I. Compositional Analysis of Root Cementum and Dentin after Er:YAG Laser Irradiation Compared with CO₂ Lased and Intact Roots Using Fourier Transformed Infrared Spectroscopy. *J. Periodontal Res.* **2002**, *37*, 50–59. [[CrossRef](#)]
52. Orsini, G.; Orilisi, G.; Notarstefano, V.; Monterubbianesi, R.; Vitiello, F.; Tosco, V.; Belloni, A.; Putignano, A.; Giorgini, E. Vibrational Imaging Techniques for the Characterization of Hard Dental Tissues: From Bench-Top to Chair-Side. *Appl. Sci.* **2021**, *11*, 11953. [[CrossRef](#)]

53. Almhöjd, U.S.; Norén, J.G.; Arvidsson, A.; Nilsson, Å.; Lingström, P. Analysis of Carious Dentine Using FTIR and ToF-SIMS. *Oral Health Dent Manag* **2014**, *13*, 735–744. [[PubMed](#)]
54. Grunenwald, A.; Keyser, C.; Sautereau, A.M.; Crubézy, E.; Ludes, B.; Drouet, C. Revisiting Carbonate Quantification in Apatite (Bio)Minerals: A Validated FTIR Methodology. *J. Archaeol. Sci.* **2014**, *49*, 134–141. [[CrossRef](#)]
55. Liu, Y.; Yao, X.; Liu, Y.W.; Wang, Y. A Fourier Transform Infrared Spectroscopy Analysis of Carious Dentin from Transparent Zone to Normal Zone. *Caries Res.* **2014**, *48*, 320–329. [[CrossRef](#)] [[PubMed](#)]
56. Bachmann, L.; Diebold, R.; Hibst, R.; Zzell, D. Infrared Spectroscopy of Dentin Irradiated by Erbium Laser. *Int. Congr. Ser.* **2003**, *1248*, 153–156. [[CrossRef](#)]
57. Spevak, L.; Flach, C.R.; Hunter, T.; Mendelsohn, R.; Boskey, A. Fourier Transform Infrared Spectroscopic Imaging Parameters Describing Acid Phosphate Substitution in Biologic Hydroxyapatite. *Calcif. Tissue Int.* **2013**, *92*, 418–428. [[CrossRef](#)]
58. Spencer, P.; Wang, Y.; Katz, J.L.; Misra, A. Physicochemical Interactions at the Dentin/Adhesive Interface Using FTIR Chemical Imaging. *J. Biomed. Opt.* **2005**, *10*, 031104. [[CrossRef](#)]
59. Villegas, M.F.; Garcia-Uriostegui, L.; Rodríguez, O.; Izquierdo-Barba, I.; Salinas, A.J.; Toriz, G.; Vallet-Regí, M.; Delgado, E. Lysine-Grafted MCM-41 Silica as an Antibacterial Biomaterial. *Bioengineering* **2017**, *4*, 80. [[CrossRef](#)]
60. Goloshchapov, D.L.; Ippolitov, Y.A.; Seredin, P.V. Mechanism of Interaction among Nanocrystalline Carbonate-Substituted Hydroxyapatite and Polar Amino-Acids for the Biomimetic Composite Technology: Spectroscopic and Structural Study. *Results Phys.* **2020**, *18*, 103277. [[CrossRef](#)]
61. Hernández, B.; Pflüger, F.; Derbel, N.; De Coninck, J.; Ghomi, M. Vibrational Analysis of Amino Acids and Short Peptides in Hydrated Media. VI. Amino Acids with Positively Charged Side Chains: L-Lysine and L-Arginine. *J. Phys. Chem. B* **2010**, *114*, 1077–1088. [[CrossRef](#)]
62. Guo, H.; Xun, Q.; Liu, S.; Wang, X. *Investigation of Ethylene Glycol Monomethyl Ether Soyate as a Biofuel*; SAE International: Warrendale, PA, USA, 2015; p. 2015–01–0955.
63. Gupta, B.S.; Jelle, B.P.; Gao, T. In Vitro Cell Composition Identification of Wood Decay Fungi by Fourier Transform Infrared Spectroscopy. *R. Soc. Open Sci.* **2022**, *9*, 201935. [[CrossRef](#)]
64. Barth, A. The Infrared Absorption of Amino Acid Side Chains. *Prog. Biophys. Mol. Biol.* **2000**, *74*, 141–173. [[CrossRef](#)] [[PubMed](#)]
65. Barth, A. Infrared Spectroscopy of Proteins. *Biochim. Biophys. Acta (BBA) Bioenerg.* **2007**, *1767*, 1073–1101. [[CrossRef](#)] [[PubMed](#)]
66. Daood, U.; Swee Heng, C.; Neo Chiew Lian, J.; Fawzy, A.S. In Vitro Analysis of Riboflavin-Modified, Experimental, Two-Step Etch-and-Rinse Dentin Adhesive: Fourier Transform Infrared Spectroscopy and Micro-Raman Studies. *Int. J. Oral Sci.* **2015**, *7*, 110–124. [[CrossRef](#)] [[PubMed](#)]
67. Ye, Q.; Parthasarathy, R.; Abedin, F.; Laurence, J.S.; Misra, A.; Spencer, P. Multivariate Analysis of Attenuated Total Reflection Fourier Transform Infrared (ATR FT-IR) Spectroscopic Data to Confirm Phase Partitioning in Methacrylate-Based Dentin Adhesive. *Appl. Spectrosc.* **2013**, *67*, 1473–1478. [[CrossRef](#)] [[PubMed](#)]
68. Khan, A.S.; Khalid, H.; Sarfraz, Z.; Khan, M.; Iqbal, J.; Muhammad, N.; Fareed, M.A.; Rehman, I.U. Vibrational Spectroscopy of Selective Dental Restorative Materials. *Appl. Spectrosc. Rev.* **2017**, *52*, 507–540. [[CrossRef](#)]
69. Nayyer, M.; Zahid, S.; Hassan, S.H.; Mian, S.A.; Mehmood, S.; Khan, H.A.; Kaleem, M.; Zafar, M.S.; Khan, A.S. Comparative Abrasive Wear Resistance and Surface Analysis of Dental Resin-Based Materials. *Eur. J. Dent.* **2018**, *12*, 057–066. [[CrossRef](#)]
70. Hędzielek, W.; Marcinkowska, A.; Domka, L.; Wachowiak, R. Infrared Spectroscopic Identification of Chosen Dental Materials and Natural Teeth. *Acta Phys. Pol. A* **2008**, *114*, 471–484. [[CrossRef](#)]
71. Uskoković, V. Visualizing Different Crystalline States during the Infrared Imaging of Calcium Phosphates. *Vib. Spectrosc.* **2020**, *108*, 103045. [[CrossRef](#)]
72. Vieira, A.A.; Silva, A.C.N. Effects of Erbium Laser Radiation on the Dentin Organic Matrix. *Laser Dent. Sci.* **2021**, *5*, 69–78. [[CrossRef](#)]
73. De Oliveira, M.T.; de Freitas, P.M.; de Paula Eduardo, C.; Ambrosano, G.M.B.; Giannini, M. Influence of Diamond Sono-Abrasion, Air-Abrasion and Er:YAG Laser Irradiation on Bonding of Different Adhesive Systems to Dentin. *Eur. J. Dent.* **2007**, *1*, 158–166. [[CrossRef](#)]
74. Torres, C.R.G.; Huhtala, M.F.R.L.; Teixeira, S.C.; Araujo, M.A.M. de Morphological Evaluation of the Bovine Dentin Prepared with High-Speed Turbine or Er:YAG Laser and Submitted to Different Adhesive Systems after Laser Etching. *World J. Dent.* **2011**, *2*, 117–123. [[CrossRef](#)]
75. Wang, K.; Yuan, Y.; Han, S.; Yang, H. Application of Attenuated Total Reflectance Fourier Transform Infrared (ATR-FTIR) and Principal Component Analysis (PCA) for Quick Identifying of the Bitumen Produced by Different Manufacturers. *Road Mater. Pavement Des.* **2018**, *19*, 1940–1949. [[CrossRef](#)]

Disclaimer/Publisher’s Note: The statements, opinions and data contained in all publications are solely those of the individual author(s) and contributor(s) and not of MDPI and/or the editor(s). MDPI and/or the editor(s) disclaim responsibility for any injury to people or property resulting from any ideas, methods, instructions or products referred to in the content.